Electronic structure of metal hydrides. V. x-dependent properties of LaH_x ($1.9 \leq x \leq 2.9$) and NdH_x ($2.01 \leq x \leq 2.27$)

D. J. Peterman
Ames Laboratory—U.S. Department of Energy and Department of Physics, Iowa State University, Ames, Iowa 50011
and Synchrotron Radiation Center, University of Wisconsin-Madison, Stoughton, Wisconsin 53589*

J. H. Weaver
Synchrotron Radiation Center, University of Wisconsin-Madison, Stoughton, Wisconsin 53589

D. T. Peterson
Ames Laboratory—U.S. Department of Energy and Department of Materials Science and Engineering, Iowa State University, Ames, Iowa 50011

(Received 10 November 1980)

The composition-dependent electronic structure of fcc LaH_x, $1.9 \leq x \leq 2.9$, has been studied using photoelectron spectroscopy with synchrotron radiation ($10 \leq h\nu \leq 50$ eV). Complementary optical reflectance measurements ($0.16 \leq h\nu \leq 4$ eV) have been performed for fcc LaH_x, $1.9 \leq x \leq 2.9$, and NdH_x, $2.01 \leq x \leq 2.27$. For LaH_x, $x \simeq 2$, the occupied d bands are ~ 1.5 eV wide and the hydrogen-induced bonding band is centered ~ 5 eV below the Fermi level, E_F (full width ~ 6 eV). Hydrogen occupation of both octahedral and tetrahedral sites is revealed for $x \leq 2$, analogous to what has been observed for other metal dihydrides. With increasing hydrogen concentration, emission from the d bands near E_F decreases and the bonding band shifts to higher binding energy; the optical spectra show a red shift of interband absorption features, increased octahedral site occupation, and increased screening of a low-energy plasmon. For LaH_x samples at the upper end of the composition range, $x \sim 2.9$, the photoemission spectra show very weak valence-band emission, and the optical spectra suggest semiconducting behavior. The binding energies of the $5p_{1/2,3/2}$ cores, E_B, measured relative to E_F are shown to increase with x (the total shift is ~ 0.8 eV for $La \rightarrow LaH_2$ and 0.9 eV for $LaH_2 \rightarrow LaH_3$). Our results are compared to band calculations by Gupta and Burger and by Misemer and Harmon and to results of NMR, specific heat, and resistivity studies.

I. INTRODUCTION

Lanthanum and neodymium hydrides, like several other rare-earth hydrides, display interesting changes in electronic structure induced by changes in hydrogen concentration. Lanthanum hydride is a particularly favorable case in which to examine these concentration dependences since the La lattice retains its fcc structure and the hydrogen atoms fill tetrahedral and octahedral sites. Early resistivity measurements by Stalinski[1] indicated that LaH_2 was a metal, that $LaH_{2.86}$ was a semiconductor, and that $LaH_{2.7}$ underwent a temperature-dependent metal-to-semiconductor transition. Bieganski and Drulis[2] reported a λ-type specific-heat anomaly at 239 K for $LaH_{2.69}$, for which the specific-heat coefficient is an order of magnitude less than that of $LaH_{2.0}$, and suggested that this change was due to a metal-to-semiconductor transition. Similar behavior was observed[2] in $NdH_{2.70}$. de Groot *et al.*[3] observed a phase transformation at 243 K in deuterium magnetic resonance studies of $LaD_{2.62}$ but saw no evidence of a metal-to-semiconductor transition although the Knight shift was quite small. Instead, they reported a structural transformation in which the La atoms were in two different environments below the transition temperature. One of these corresponded to the $LaH_{2.5}$ structure suggested earlier through neutron diffraction results[4] while the other was of a higher symmetry with La atoms having four rather than three nearest-neighbor deuterium atoms. Neutron-diffraction results[4] indicated a tetragonal distortion in LaD_x and CeD_x for hydrogen to metal ratios, x, of ~ 2.3.

The properties of LaH_x are similar in many respects to those of the much-studied CeH_x system (CeH_x is also fcc for $2 < x < 3$). Resistivity measurements[5] have provided evidence of a composition-

dependent metal-to-semiconductor transition at about $x = 2.8$. As with LaH_x, this transition is temperature dependent for $2.7 \leq x \leq 2.8$. Libowitz *et al.*[6] determined the transition temperature to be 245 K for $CeH_{2.77}$ and 255 K for $CeH_{2.86}$. Their x-ray-diffraction studies showed a tetragonal distortion occurring near 245 K for $CeH_{2.75}$. A semiconductor band gap of 0.104 eV has been reported[7] for $CeH_{2.81}$.

Band-structure calculations by Switendick[8] for the YH_0-YH_1-YH_2-YH_3 series were the first to explain the electronic structure of hydrides, including the metal-to-semiconductor transition, without evoking the protonic or anionic models. His work showed that new bands were added below E_F as hydrogen was added and that there was considerable hybridization between the metal and hydrogen electronic states. Kulikov and Zvonkov[9] presented the first band-structure calculations of LaH_2, LaH_3, CeH_2, and CeH_3. Gupta and Burger[10] have recently reported non-self-consistent augmented plane-wave (APW) calculations for LaH_2 and LaH_3, and self-consistent Korringa-Kohn-Rostoker (KKR) calculations by Misemer and Harmon are now in progress.[11] Our work with several lanthanide hydrides[12–19] and, in particular, our previous studies[12–15] of ScH_2 and YH_2 have strongly supported the band-structure results.

The present study was undertaken to examine near-stoichiometric LaH_2 and LaH_3 and to go a step further by studying the x-dependent electronic structure in the intermediate composition range. Additional studies were performed with NdH_x ($2.01 \leq x \leq 2.27$) to gain further insight into the electronic-structure changes near the dihydride limit. Our results not only test the calculated bands of LaH_2 and LaH_3 (more complicated than those of ScH_2 and YH_2 due to relativistic effects), but also reveal some interesting x dependences which should stimulate further theoretical efforts.

In the following we present the experimental details, results, and conclusions of our photoemission and optical studies. We begin by describing our sample preparation and measurement techniques in Sec. II (see Papers I and III of this series for a more comprehensive introduction to optical and photoemission spectroscopies, particularly as they have been applied to hydride systems). The experimental results[19] are presented in Sec. III. In Sec. IV we relate our results to the previously mentioned studies of LaH_x, discussing the implications for the concentration-dependent metal-semiconductor transition.

II. EXPERIMENTAL DETAILS

The samples used in this study were prepared in bulk form starting with polycrystalline La or Nd. The high-purity Ames Laboratory lanthanum and neodymium typically contained less than 20 atomic parts per million (ppm) total metallic impurities and 250, 30, and 93 at. ppm of O, N, and C for La and 360, 21, and 84 at. ppm of O, N, and C for Nd. In preparation for hydrogen charging, slices of metal were electropolished in a perchloric acid solution (6% by volume in methanol at ~200 K). They were then wrapped in tantalum foils and heated under vacuum in the hydrogen charging apparatus to 850 °C (800 °C for Nd) to outgas the metal and increase the surface permeability to hydrogen. The tantalum minimized contamination from the quartz or stainless-steel furnace tubes by reacting with carbon or oxygen. A mixture of hydrogen and helium gases was used for low-pressure hydrogen charging; helium served to moderate the rate of hydrogen uptake and made it possible to synthesize large, bulk samples free of cracks and voids. Samples of LaH_x with hydrogen concentrations greater than 2.7 were first formed at low pressure to form a low-x hydride, reheated to ~500 °C and exposed to hydrogen pressures of up to 150 atm. All samples were analyzed for hydrogen concentration by a hot-vacuum extraction technique with an estimated accuracy of ~2%.

For photoelectron spectroscopy, samples were cut to $\sim 3 \times 3 \times 12$ mm^3 and attached to copper sample holders in an argon glove box. Since these samples were to be fractured *in situ* in the photoemission chamber, no further surface preparation was required.

The photoemission measurements were performed at the Synchrotron Radiation Center of the University of Wisconsin using radiation emitted by 240-MeV electrons orbiting in the electron storage ring Tantalus. These experiments were done at room temperature using radiation dispersed by a uhv 3-m toroidal grating monochromator ($10 \leq h\nu \leq 50$ eV). A double-pass cylindrical mirror analyzer was used to detect the emitted electrons. The overall resolution (electrons plus photons) was 0.4–0.6 eV. The experimental geometry has been discussed elsewhere.[20] Many samples, each attached to a copper holder, were loaded onto a sample bank in the photoemission chamber for extended runs. The samples were fractured *in situ* at operating pressures of $5–8 \times 10^{-11}$ Torr (base pressure $\sim 3 \times 10^{-11}$ Torr) and translated immediately to the mutual focus of the analyzer and the radiation beam. No pressure bursts, which would indicate the escape of hydrogen from the hydride, were observed with any sample at the moment of fracture. There was no evidence of sample degradation due to hydrogen loss after cleaving; LaH_x samples of high x aged *in situ* overnight did show contamination features at ~9.5 eV below E_F.

Samples for optical spectroscopy were cut to $\sim 2 \times 8 \times 8$ mm^3 and polished by wet grinding with alumina abrasives through 0.3 μm (Linde *A*). They were ultrasonically cleaned in methanol, dried using high-purity nitrogen, and transferred to the experi-

mental apparatus as quickly as possible to minimize exposure to moist laboratory air (within ~5 min the sample was inside the N_2-purged measurement chamber; evacuation of the chamber began after another ~5 min).

The optical absorptivity ($A = 1 - R$ where R is the reflectivity) was measured at 4.2 K in the photon energy range $0.16 \leq h\nu \leq 4.0$ eV. Monochromatic radiation was focused onto the sample at near-normal incidence. Part of the beam was absorbed and part reflected onto a gold-black coated absorber (absorptivity ~100% in our spectral range). Both elements experienced increases in temperature (~mK above ambient) due to the absorption of microwatts of radiant energy. Joule heating in matched 1000-Ω metal heaters was used to duplicate the temperature excursion. The power required for that duplication was then measured and the absorptivity was calculated directly. This calorimetric method, as we have termed it, makes it possible to measure A with an accuracy of approximately 1–2% depending on the total light intensity (i.e., the temperature excursions of sample and absorber), as discussed in detail elsewhere.[21]

III. RESULTS AND DISCUSSION

A. Photoelectron spectroscopy

Photoelectron energy distribution curves (EDC's) for $LaH_{1.98}$, $LaH_{2.48}$, and $LaH_{2.89}$ are shown in Figs. 1–3. A sequence of EDC's taken at different photon energies, $h\nu$, for $11 \leq h\nu \leq 50$ eV, is shown for each hydrogen composition in Figs. 1(a)–1(c). In each case, the number of photoelectrons is plotted in arbitrary units and the electron initial-state energy is referenced to the Fermi level E_F ($x = 1.98, 2.48$) or the top of the valence band E_V ($x = 2.89$). The spectra in Fig. 2 ($h\nu = 40$ eV) have been normalized to the integrated emission from the La $5p_{1/2}, 5p_{3/2}$ doublet. The energy distribution curves in Fig. 3 ($h\nu = 19$ or 20 eV) have been redrawn for comparison to each other and to the calculated state densities.[10,11]

The spectra for $LaH_{1.98}$ [Fig. 1(a)] show features which are typical of all metallic dihydrides. In Fig. 4 we reproduce the self-consistent energy bands calculated[13] for YH_2. The calculated density of states is shown alongside the bands. The relatively narrow band of emission shown in Fig. 1(a) within 1.5 eV of E_F reflects the width of the occupied metal d band. The shoulder at −0.6 eV can be associated with the relatively flat portion of that band in the symmetry direction $K_1 \rightarrow W_2'$ and is analogous to that observed in ScH_2 at −0.8 eV, YH_2 at −1.1 eV, and LuH_2 at −1.1 eV. The deeper band of emission reflects the hybridized (sp-d) covalent bonding bands. As Switendick first pointed out,[8,12–19] these bands result from the interaction of bonding and antibonding combinations of H-derived orbitals with metal states of the appropriate symmetry; some metal states are lowered 5–10 eV by the M-H interaction.

The density of states (DOS) for LaH_2 is shown

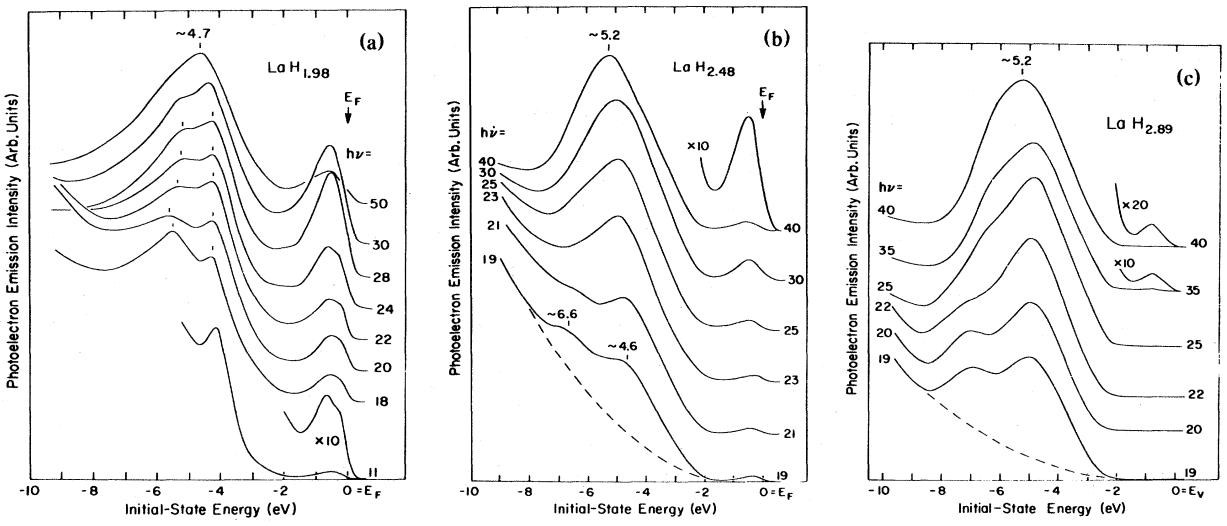

FIG. 1. (a) Photoelectron energy distribution curves (EDC's) for $LaH_{1.98}$ showing the electronic emission as a function of initial-state energy referenced to the Fermi level, E_F. The feature within ~2 eV of E_F is derived primarily from La d-like states and is termed the metal band in the text. The deeper emission feature, termed the bonding band in the text, is derived from bands with mostly hydrogen s character which are hybridized with metal s-, p-, and d-like states. (b) Photoelectron EDC's for the intermediate concentration $LaH_{2.48}$ showing the diminished metal band near E_F and the bonding band shifted to higher binding energy. (c) Photoelectron EDC's for $LaH_{2.89}$ showing very weak valence-band emission. As discussed in the text, the energy zero is taken to be the top of the valence band for $LaH_{2.89}$.

dashed in Fig. 3 (Gupta and Burger from their non-self-consistent APW band calculations). The two large peaks in the DOS were associated[10] with the flat bands near K_1, X_3, and L_1 and flat bands near W_3 and along Σ_3. The composite or double-structured character of the bonding band of $LaH_{1.98}$ arises from those features in the density of states. Each feature contains primarily hydrogen s character but also significant metal s, p, and d character. The calculated DOS peak near −4.5 eV agrees quite well with experiment and the deeper peak near −5.4 eV is also in rather good agreement. However, the calculated full width at half maximum of the DOS (~1.7 eV) is considerably less than experiment indicates (~3.5 eV). The calculations of Kulikov and Zvonkov[9] place their bonding band center too close to the Fermi level (~2.5 eV below E_F).

In general, theory places the bottom of the bonding band too close to E_F and underestimates its width. As shown in Fig. 3, the experimental bonding band extends to about −8.5 eV compared to −6.7 eV (Gupta and Burger[10]) and −5.4 eV (Kulikov and Zvonkov[9]). As has been shown for ScH_2 and YH_2,[13,15] there are calculational refinements which improve agreement of theory with experiment, e.g., self-consistency and a better treatment of the octahedral potential.

The experimental feature near −5.5 eV [Fig. 1(a)] is clearly visible for $h\nu \approx 18$ eV, but eventually disappears above $h\nu = 30$ eV. It can be associated with low angular momentum states; the decrease of the photoionization cross section with increasing photon energy is discussed, for example, by Manson.[22,23] That interpretation is supported by angular momentum projections of the wave-function character of the calculated bands; Fig. 7 of Ref. 10 shows a La s-like peak ~0.2 eV below the peak at −5.6 eV.

In Fig. 1(b) we show a series of EDC's for $LaH_{2.48}$, i.e., a composition intermediate between the cubic dihydride and the cubic trihydride. Comparison to the photoemission spectra for $LaH_{1.98}$ shows that the d-band emission within ~1.5 eV of E_F has dimin-

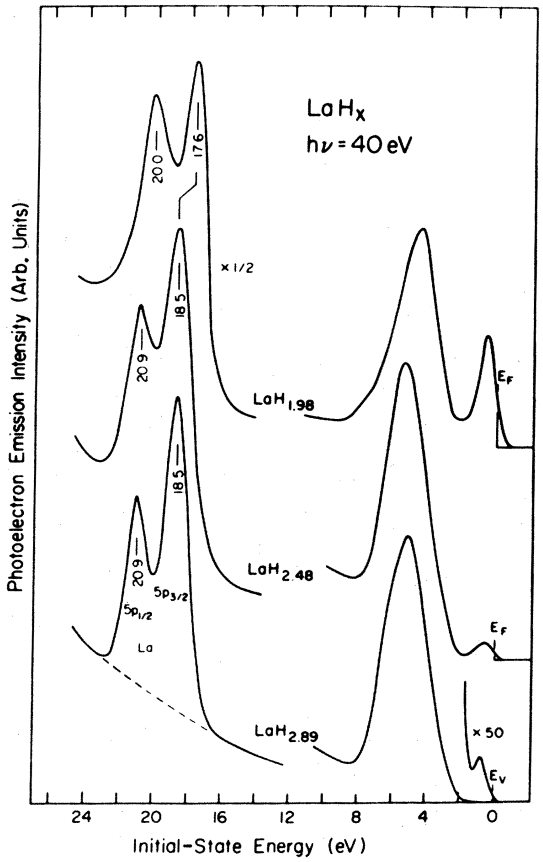

FIG. 2. Photoelectron EDC's for $h\nu = 40$ eV for $LaH_{1.98}$, $LaH_{2.48}$, and $LaH_{2.89}$ normalized to the emission from the La $5p$ core levels. As x increases, the binding energies of the cores increase, the d-band emission decreases and the bonding band shifts to higher binding energy.

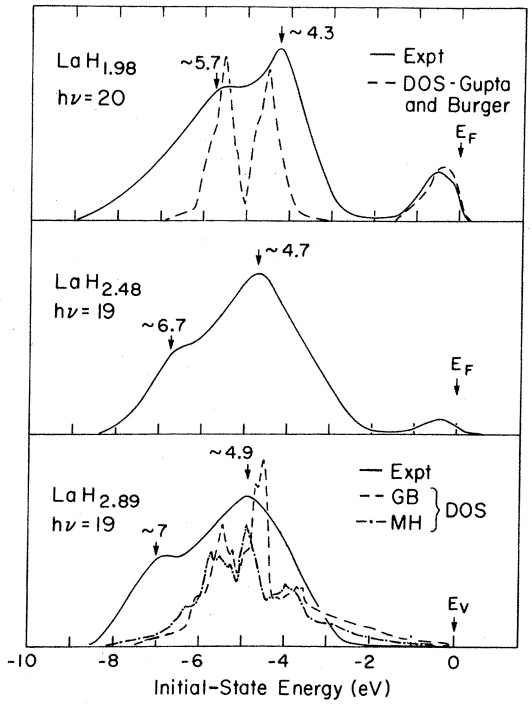

FIG. 3. Photoelectron EDC's for $LaH_{1.98}$, $LaH_{2.48}$, and $LaH_{2.89}$ with background subtracted compared to calculated densities of states for LaH_2 and LaH_3 (Gupta and Burger) and LaH_3 (Misemer and Harmon). The calculated bonding band centers agree with experiment, but their widths are significantly narrower. As discussed in the text, the deepest-lying features which are enhanced at these photon energies show the most $h\nu$ dependence, reflecting the photoionization cross section of low angular momentum states (most likely La s-like).

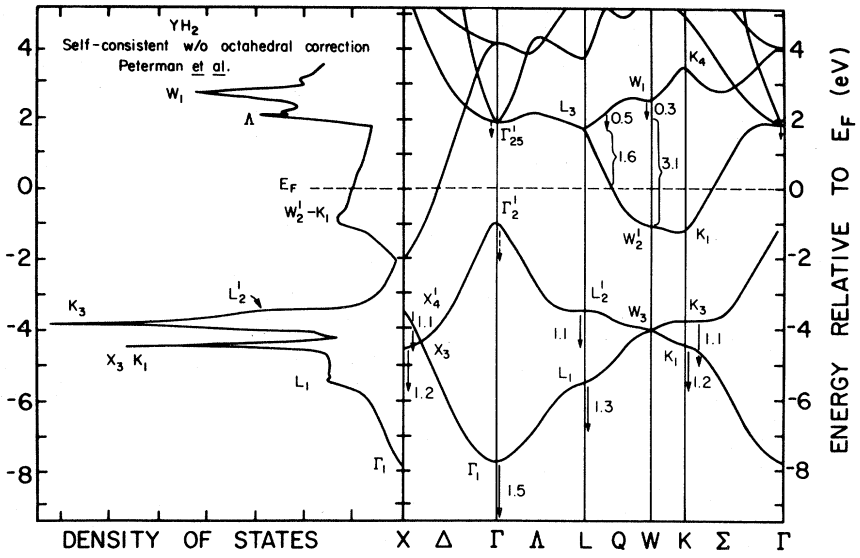

FIG. 4. Self-consistent KKR energy bands and density of states (DOS) of YH_2 (Ref. 13). The arrows in the bands represent the corrections indicated by photoemission and optical experiments. Similar changes can be anticipated for LaH_2. This "representative" dihydride band structure shows the origin of the metal band ($W_2' - K_1$) and the bonding band; symmetry directions and points in the dihydride bands are referred to in the text.

ished by a factor of ~6–8 (spectra normalized to La $5p$ cores). The features in the bonding band have shifted to higher binding energies (bonding band center ~5.2 eV below E_F for $LaH_{2.48}$ vs ~4.7 eV for $LaH_{1.98}$). As with $LaH_{1.98}$, the contribution of the low angular momentum states to the EDC's is visible at low photon energies.

The EDC's for $LaH_{2.89}$ [Fig. 1(c)] show that there is only very weak emission within ~2 eV of E_F. The emission strength of that feature is reduced by a factor of 200–400 relative to that of $LaH_{1.98}$ ($h\nu = 30$- and 40-eV spectra normalized to La $5p$ core emission). The choice of the energy zero was dictated by studies of the La $5p$ core levels (Fig. 2). For $LaH_{1.98} \rightarrow LaH_{2.48}$ there is a binding energy shift of 0.9 eV (core energies measured relative to E_F). For $LaH_{2.48} \rightarrow LaH_{2.89}$, one would expect either a further increase in binding energies or no shift at all but not a decrease. Alignment of the spectra for $LaH_{2.89}$ keeping the core energies fixed places the zero as shown in Fig. 2, and it appears that zero corresponds to the top of a weakly emitting semiconductor valence band. If the hydride were taken to be metallic, then E_F would be halfway up the emission onset, indicating a decrease of E_B by 0.3–0.4 eV and the binding energies would be intermediate between those of $LaH_{1.98}$ and $LaH_{2.48}$. Our identification of $LaH_{2.89}$ as a semiconductor is consistent with recent resistivity measurements by Finnemore *et al.*[24]

The emission features of the bonding band for $LaH_{2.89}$ retain some similarities to those of $LaH_{1.98}$ and $LaH_{2.48}$. The center falls ~5.2 eV below E_V with a full width of ~6 eV. The location of the bonding band center represents an independent argument for the energy scale shown since, if $LaH_{2.89}$ was treated as metallic, its bonding band center would be closer to E_F than for $LaH_{2.48}$ and comparable to that of $LaH_{1.98}$. Again, at lower photon energies, a peak associated with low angular momentum initial states is visible at −7 eV. For $h\nu = 40$ eV, it has disappeared and we observe only a relatively broad emission band.

Two calculated[10,11] densities of states for LaH_3 are shown in Fig. 3 for comparison to the experimental spectra of $LaH_{2.89}$ taken at $h\nu = 19$ eV. The calculations indicate a broad bonding band centered ~5 eV below E_F and show no peak at −7 eV. Again, there is a La s-like peak in the projected DOS ~1 eV below the central peak[11] from which emission is presumably enhanced at low photon energy. The discrepancy of ~1 eV is typical for differences observed in ScH_2 and YH_2 between the energy of the deepest bonding band shoulder and the calculated band with which it must be associated (L_1, K_1, and nearby volumes of $\vec{k}$ space).

B. Optical spectroscopy

The absorptivity spectra for samples of LaH_x ($x = 1.9$, 2.04, 2.15, 2.36, ~2.45, 2.63, 2.67, and 2.87) and NdH_x ($x = 2.01$, 2.21, and 2.27) are shown in Figs. 5 and 6 as measured at 4.2 K at near-normal incidence. For clarity the spectra have been displaced upward in units of 0.1 or 0.2 with increasing x;

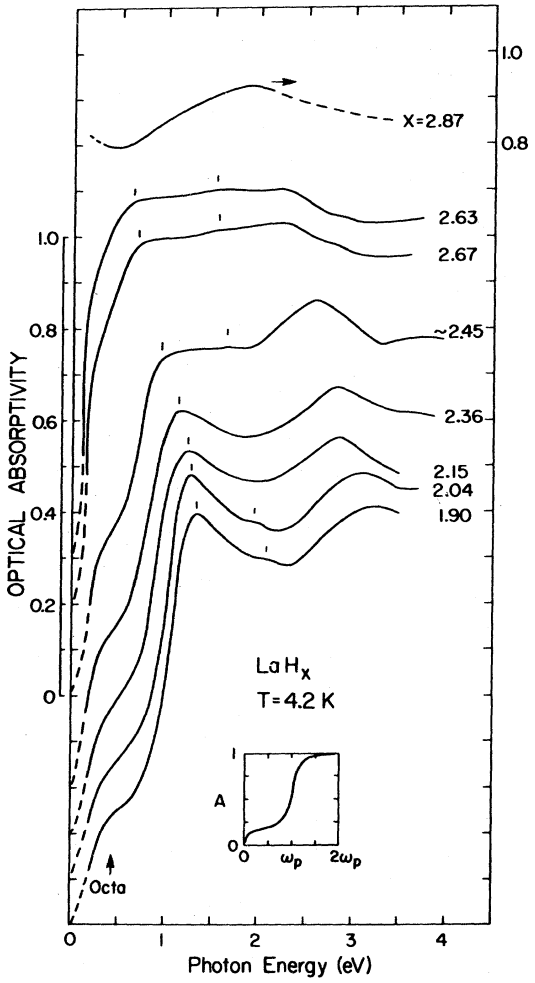

FIG. 5. Optical-absorptivity spectra for LaH_x for a range of hydride compositions. The spectra are displaced upward for clarity, the dashed lines at low energy guide the eye to the respective zeros, and the scale is given alongside the figure. The dashed lines below 0.25 and above 2.2 eV for $LaH_{2.89}$ reflect greater experimental uncertainty with that sample of high hydrogen concentration. With increasing hydrogen, the interband feature labeled "octa" grows in strength while higher-energy interband structures red shift with increasing x. The inset shows a model calculation for the absorptivity of a free-electron metal. Deviations in the real spectra are due to interband absorption.

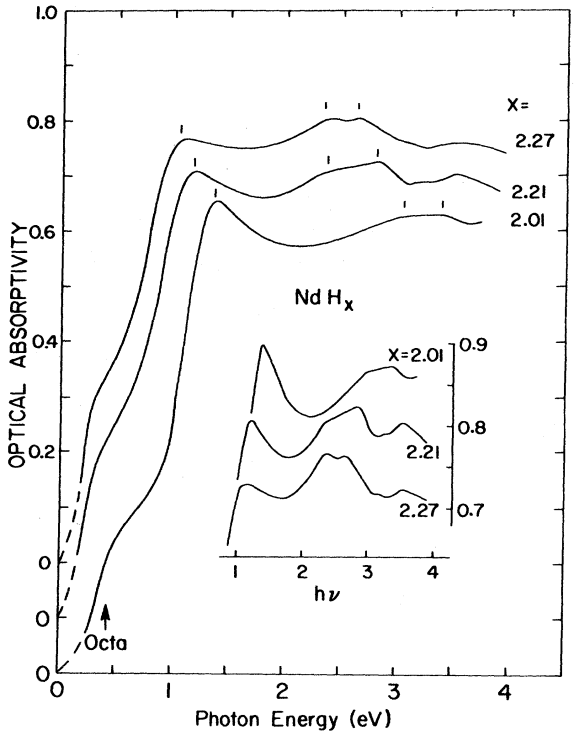

FIG. 6. Optical-absorptivity spectra for NdH_x for compositions near $x=2$. As with LaH_x, increasing the hydrogen concentration shifts interband features to lower energy, increases the strength of the octahedral feature, and screens the plasmon.

dashed curves at low photon energy guide the eye to the respective zeros. For $LaH_{2.63}$ and $LaH_{2.67}$, the ordering of the spectra was dictated by trends in the absorptivity spectra themselves rather than in hydrogen composition analysis. This is consistent with the -2% uncertainty in determining x. For $LaH_{2.87}$, the absorptivity scale is indicated at the right of the figure and no extrapolation to zero is drawn. The curve for $LaH_{2.87}$ is drawn dashed above 2.2 and below 0.25 eV because of greater experimental uncertainty in the data for that sample. For NdH_x, the energy range of 1–4 eV is expanded in the inset of Fig. 6.

The concentration-dependent absorptivity spectra of LaH_x appear to fall in three types. In Fig. 5 the similarities for $x=1.9$, 2.04, 2.15, and 2.36 are quite apparent. However, the spectra for $x\simeq 2.63$ and $x=2.87$ differ from each other and from the lower-x spectra, most notably at low photon energies ($h\nu \leq 1$ eV). The samples themselves also seemed to fall into three groups: while it was relatively easy to synthesize hydrides with concentrations of approximately 2.0, 2.6, and 2.9, it was more difficult to obtain intermediate concentrations. (Indeed, the $x\simeq 2.45$ spectrum was measured using a sample of nominal concentration of 2.15 which was electropolished; electropolishing had the effect of increasing the hydrogen content within the optical penetration depth.)

The absorptivity spectra for LaH_x, $x\simeq 2$, are typical of dihydrides of Sc, Y, and other lanthanides.[12,18] For each, the absorptivity is relatively low at low photon energy, it increases sharply to $A\approx 0.8$ between 1 and 2 eV, and interband structures are observed at higher energy. The increase or edge corresponds to the plasma energy, the energy at which a propagating charge would induce a resonant electronic response,

and is typical of materials with only a partially occupied band near E_F. Such materials typically have interband absorption edges near 1–2 eV and are strikingly colorful because of reflectance changes in the visible part of the optical spectrum; for example LuH_2 is blue in color.

When only tetrahedral sites are occupied in the CaF_2 dihydride lattice, there are no interband structures below the plasmon edge[12,16] and the absorptivity can be described by a Drude or free-electron model. Well below the plasma frequency, the absorptivity is small and nearly constant. In the inset of Fig. 5 we show a model calculation for A vs $\hbar\omega$ in units of $\hbar\omega_p$ for a free-electron metal. The behavior of $ScH_{1.61}$ below the experimental interband onset and the plasmon edge ($\sim$1.5 eV) is described quite well by such a model; it fails for LaH_x because of the low-energy feature labeled "octa" in Fig. 5.

For most dihydrides, there is structure below the plasmon edge which is visible in the absorptivity at about 0.5 eV (see Fig. 5 for LaH_x and Fig. 6 for NdH_x). We postulated[12,13] that this structure indicated occupation of octahedral sites before all tetrahedral sites were filled. Neutron diffraction,[25] NMR,[26] and ESR[27] studies have confirmed that interpretation. Band calculations[28] of ordered Y_4H_9 and Y_4H_{11} suggest that octahedral occupation does modify the band structure sufficiently for new low-energy interband transitions to occur. The departure of the experimental spectra for LaH_x, $x \simeq 2$, from the free-electron behavior reflects the optical transitions due to occupied octahedral sites.

LaH_x has the largest lattice constant of the cubic dihydrides ($a_0 = 5.65$ Å) and the octahedral sites appear to be occupied "more prematurely" in LaH_x than in the more compact dihydrides of yttrium ($a_0 = 5.20$ Å) or scandium ($a_0 = 4.80$ Å). As the results for LaH_x show (Fig. 5), the octahedral feature becomes more prominent with increasing hydrogen concentration and the edge near 1 eV shifts to lower energy. Similar behavior is shown in Fig. 5 for NdH_x ($x = 2.01$, 2.21, and 2.27). With increasing hydrogen concentration, the octahedral feature increases and the plasmon is shifted to lower energy and broadened (screened).

The results of Figs. 5 and 6 show that the interband absorption features also shift to lower energy as x increases. The doublet (minimum) near 2.2 eV shown in Fig. 5 for $LaH_{1.9}$ corresponds to a maximum in the interband absorption. That minimum red shifts with x ($\sim$2.2 eV at $x = 1.9$; $\sim$1.9 eV at $x = 2.36$; nearly absent for $x \simeq 2.45$). The results for NdH_x (Fig. 6) show similar behavior and it appears to be a general x-dependent property. It is important to note that for NdH_x the optical interband features near 2.5-eV red shift but do not significantly broaden as the amount of disorder increases (for $NdH_{2.27}$ there is at best $\sim$27% occupation of O sites and 100% occupation of T sites; it is more likely, however, that there are 0–10% T-site vacancies and 27–40% O-sites occupancy[29]). The interband features are similar to those observed in ScH_x, YH_x, GdH_x, TbH_x, ErH_x, and LuH_x and arise from electronic transitions between d-like bands, specifically along Q, W-K, and Σ. Differences between the optical spectra of these dihydrides can thus be related, to first order, to the width of the elemental d bands. These bands are largely d derived and are apparently insensitive to disorder on the H sublattices at these concentrations.

At high hydrogen concentrations, $LaH_{\sim 2.6}$, the octahedral features dominate the low-energy absorptivity spectrum and a plasmon edge cannot be identified. For $LaH_{2.87}$ (uppermost curve, Fig. 5), the resemblance to $LaH_{1.9}$ is almost completely lost. Instead, the absorptivity is nearly constant in magnitude ($A = 0.80$) below $\sim$0.8 eV and shows no free-electron edge (for metals one should see $A \simeq 2/\omega_p\tau$ and ultimately $A \to 0$ as $\hbar\omega \to 0$). Indeed, for LaH_x the absorptivity seems to increase near the low-energy limit of our measurements. The absence of the free-electron edge indicates that $LaH_{2.87}$ is semiconducting at $T = 4.2$ K.

A more quantitative comparison of theory with experiment comes through considerations of features in ϵ_2, the imaginary part of the dielectric function, as discussed in Ref. 12. To determine ϵ_2 from the absorptivity spectra, Kramers-Kronig (KK) integrals have been evaluated. The extrapolations outside the range of measurements were guided by reflectance measurements of ScH_2 for $4 \leq h\nu \leq 25$ eV; above 25 eV they were based on a power law of the form $R = R_0 E^{-3.5}$. The infrared extrapolation was based on a Drude behavior and was relatively straightforward for LaH_x, $1.9 \leq x \leq 2.6$, and for NdH_x.

The infrared extrapolation for $LaH_{2.87}$ was more uncertain. While a Drude model is sufficient for a metal, for a semiconductor a variety of low-energy mechanisms contribute to the infrared absorption spectra. For example, the absorption coefficient, $\alpha = \epsilon_2\omega/nc$, has been shown to vary as $\omega^{-3/2}$ for scattering by acoustical phonons, as $\omega^{-5/2}$ for scattering by optical phonons, and as ω^{-3}–$\omega^{-3.5}$ for scattering by ionized impurities.[27] In general, the dominant mode of scattering depends on the impurity concentration. Furthermore, at sufficiently low energy the reflectance spectrum has structure related to the lattice vibrational modes. Nonetheless, for $LaH_{2.87}$ the use of two very different extrapolations for the absorptivity, one a constant and the other a rapidly decreasing exponential, led to relatively small differences in the dielectric functions at photon energies greater than $\sim$0.6 eV.

These extrapolations are, of course, not unique. Experience has shown that while the magnitudes of the calculated dielectric functions will change by 10–20%, the shapes and particularly the energy loca-

tions of interband features do not. Our primary interest is in the shapes and the energy locations of the various interband transition maxima for comparison to band calculations.

The real and imaginary parts of the dielectric functions, $\epsilon_1(\omega)$ and $\epsilon_2(\omega)$, derived by KK analysis from the absorptivity spectra of LaH_x are shown in Fig. 7 and the optical conductivities, $\sigma = \epsilon_2\omega/4\pi$ are shown in Fig. 8. In Fig. 9 we show the dielectric functions for NdH_x.

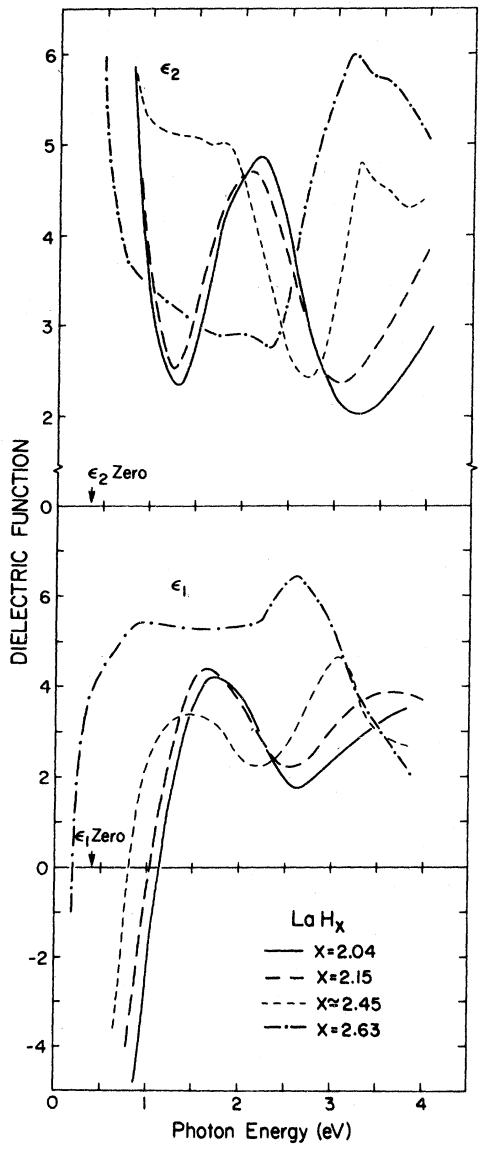

FIG. 7. Real and imaginary parts of the dielectric function $[\tilde{\epsilon}(\omega) = \epsilon_1 + i\epsilon_2]$ for LaH_x. The interband onset for $LaH_{2.04}$ is 1.1 ± 0.1 eV. Below 1 eV, the low-x spectra are dominated by free-carrier effects which diminish in importance with increasing x. Structure in ϵ_2 is related to interband absorption as discussed in the text.

The x dependence of the octahedral feature is revealed best through the conductivity spectra (Fig. 8). An estimate of its strength for $LaH_{2.04}$ is shown dashed in Fig. 8; that curve was obtained by subtracting a free-carrier background (dashed line). The octahedral feature for $LaH_{\sim 2.45}$ is considerably stronger and the free-carrier contribution is diminished. For higher x, the conductivity spectra show further loss in free-carrier absorption.

In Fig. 8, the interband onset (neglecting the "octa" contribution) in $LaH_{2.04}$ is shown to be 1.1 ± 0.1 eV (dashed curve). The interband structure at higher energy is centered at ~2.3 eV and is a composite structure (peak at 2.3 eV, shoulder at ~1.8–1.9 eV). By analogy to YH_2 this interband onset corresponds to optical transitions which occur along the symmetry direction Q between L and W. This identification is in good agreement with the cal-

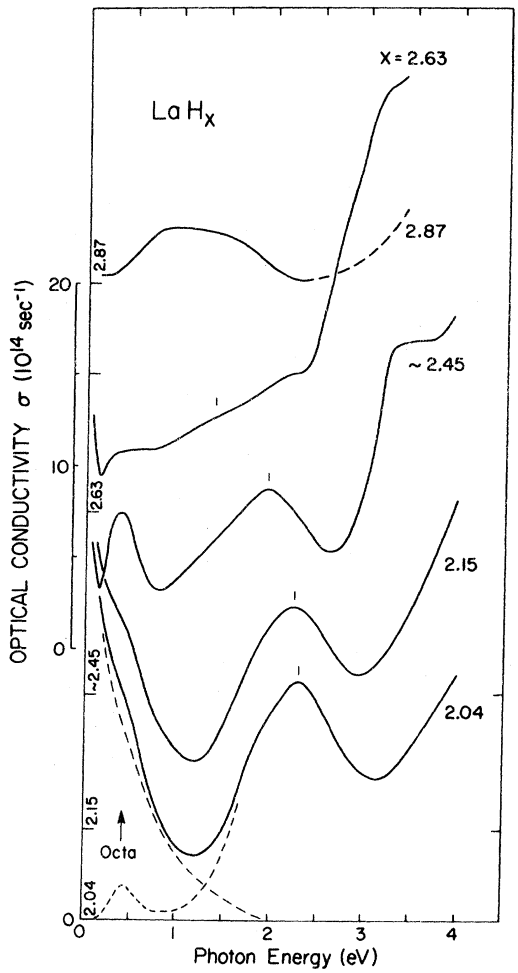

FIG. 8. Optical conductivity, $\sigma = \epsilon_2 E/4\pi\hbar$, for LaH_x. The octahedral feature is shown at 0.4 eV and its strength increases with x. Interband features (onset ~1.1 eV for $LaH_{2.04}$) shift to lower energy with increasing x.

culations by Gupta and Burger[10] (calculated onset ~1.3 eV) but there is less satisfactory agreement with those of Kulikov and Zvonkov[9] (onset ~3 eV near Γ).

The center of the prominent $LaH_{2.04}$ interband structure seen in ϵ_2 or σ is at ~2.2 eV. For $ScH_2 \rightarrow YH_2$ the analogous structure shifts to higher energy (~2.4 → 2.8 eV) and broadens,[12] an effect which can be related to the increased width of the elemental metal *d* bands upon going from 3*d* to 4*d* transition metals.[30] That this structure in LaH_2 appears at *lower* energy and is narrower can be related to lattice size and *d*-band overlap: the LaH_2 lattice is significantly larger, in comparison to that of ScH_2 and YH_2, than would be anticipated by comparing the elemental metal lattices, and the LaH_2 *d*-derived bands are thus narrower. This narrowing can also be seen experimentally in the photoemission results (Figs. 1–3) where a shoulder related to the band along *W*-*K* was observed at −0.6 eV.

The relatively broad feature in σ centered at ~1.1 eV for $LaH_{2.89}$ (Fig. 8) can be associated with transitions occurring over a substantial volume of $\vec{k}$ space extending outward from the center of the Brillouin zone. The trihydride calculations[9–11] indicate that such transitions are possible along Γ-Λ-*L* between bands 3 and 4, where Γ_1 is the top of the valence band. Furthermore, an increase in ϵ_2 or σ (near 2.3 eV shown dashed in Figs. 7 and 8) is expected when the $L_2' \rightarrow L_3$ interband transition threshold is reached. This threshold occurs at ~2.3 eV in the calculations of Misemer and Harmon.[11]

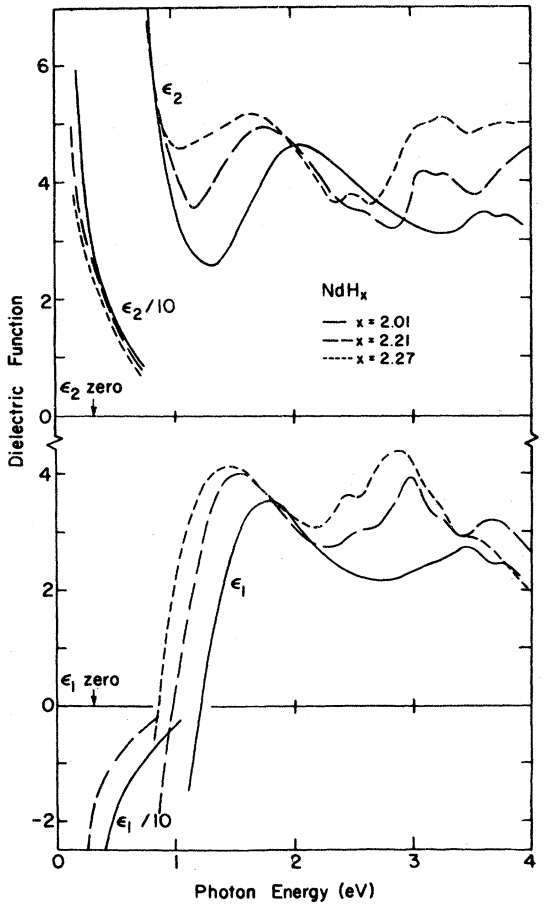

FIG. 9. Dielectric functions for NdH_x showing effects similar to those observed for LaH_x.

IV. CONCLUSIONS

The photoelectron and optical spectroscopy results presented here support the results of recent band-structure calculations for LaH_2-LaH_3 by Gupta and Burger[10] and those of the self-consistent calculations for LaH_3 by Misemer and Harmon.[11] The energy discrepancies between the theoretical peak positions and those observed in the photoemission experiments are not serious considering the sensitivity of states with high hydrogen character to the choice of muffin-tin radii.[31] The overall trends in going from LaH_2 to LaH_3 predicted by Gupta and Burger are reproduced. Specifically, the center of the bonding bands shifts less than 0.6 eV to higher binding energy and the metal-like states below E_F in the dihydride are lowered, causing the *d*-like peak just below E_F in the LaH_2 photoemission spectra to diminish with increasing *x*. There is less satisfactory agreement with the calculations of Kulikov and Zvonkov where for $LaH_2 \rightarrow LaH_3$ the center of the bonding bands was lowered by about 3 eV (from ~2.5 to ~5.4 eV below E_F).

For LaH_3, the various calculations disagree as to whether LaH_3 is a semiconductor or a semimetal. Gupta and Burger calculated a direct gap of 0.53 eV ($\Gamma_1 - \Gamma_{25}'$), Kulikov and Zvonkov predicted an indirect band overlap of ~0.4 eV (Γ_1-L_3), and Misemer and Harmon showed an overlap of less than 0.05 eV. Our optical and photoemission results suggest that LaH_3 is a semiconductor, in agreement with recent resistivity measurements.[24]

The small specific-heat coefficient of $LaH_{2.69}$ relative to LaH_2 can be adequately explained by the much smaller density of states at E_F as suggested by our photoemission results (e.g., Fig. 2). We have seen that $LaH_{\sim 2.5}$ is metallic at room temperature but the *d*-band emission is reduced by a factor of ~6–8 relative to that of LaH_2. The residual free-carrier contribution to the absorptivity spectra of samples of this concentration indicate that they are metallic at 4.2 K.

In our interpretation of the photoemission and optical results we have been guided by calculations for ordered, stoichiometric dihydrides and trihydrides. While these are sufficient for understanding the

behavior near $x=2$ and 3, the observed x dependences are difficult to interpret within this relatively limited theoretical framework. For example, the rapid decrease in the d-derived density-of-states-like initial-state features observed in photoemission spectra can be qualitatively understood from band calculations which show strong d character near E_F at $x=2$ but not for $x=3$. At the same time, we see an increase in the octahedral site interband feature as x increases above $x=2$. However, we also see a red shift of optical features with increasing x and this is more difficult to understand. Since the lattice contracts with the addition of hydrogen, one might rather expect a blue shift due to the widening d bands. A similar blue shift would accompany the drawing away from E_F of the occupied d states as the dihydride converts to the trihydride. A band calculation of ordered LaH_x with intermediate composition is necessary to understand the observed red shift of the interband feature. Such a calculation also represents a logical theoretical step and will lead to a better understanding of the many experiments that have dealt with the electronic properties of these hydrides.

ACKNOWLEDGMENTS

The authors gratefully acknowledge many stimulating discussions with D. Misemer, B. N. Harmon, D. G. de Groot, R. G. Barnes, N. I. Kulikov, and D. W. Lynch. We thank M. Gupta and J. P. Burger for an unpublished report of their LaH_2 and LaH_3 calculations. The technical support of A. D. Johnson and H. H. Baker in preparing and handling these fragile samples was invaluable, as was the generous support of the staff of the Synchrotron Radiation Center and the Ames Laboratory. This work was supported by the U. S. DOE (Contract No. W-7405-Eng-32 to the Ames Laboratory and Contract No. DE-AC02-80ER10584 to Wisconsin). The Synchrotron Radiation Center is operated with NSF support under Grant No. DMR78-21888.

---

*Present address.

[1]B. Stalinski, Bull. Acad. Pol. Sci. Cl. 3: 5, 1001 (1957).

[2]Z. Bieganski and M. Drulis, Phys. Status Solidi (a) 44, 91 (1977).

[3]D. G. de Groot, R. G. Barnes, B. J. Beaudry, and D. R. Torgeson, Hydrogen in Metals Conference, Münster, 1979 (unpublished); Z. Phys. Chem. Neue Folge, Bd. 116, (1979).

[4]C. G. Titcomb, A. K. Cheetham, and B. E. F. Fender, J. Phys. C 7, 2409 (1974).

[5]B. Stalinski, Bull. Acad. Pol. Sci. Ser. Sci. Chim. 76, 837 (1972).

[6]G. G. Libowitz, J. G. Pack, and W. P. Binnie, Phys. Rev. B 6, 4540 (1972).

[7]G. G. Libowitz, Ber. Bunsenges. Phys. Chem. 76, 837 (1972).

[8]A. C. Switendick, Int. J. Quantum Chem. 5, 459 (1971).

[9]N. I. Kulikov and A. D. Zvonkov, Z. Phys. Chem. 116, 479 (1979). Their results for ScH_2 and YH_2 can be compared with the non-self-consistent band calculations in Refs. 8 and 13, the self-consistent results in Ref. 13, and the experimental results in Refs. 12 and 14. Apparently their early model Hamiltonian method was not as accurate as the APW or KKR methods.

[10]M. Gupta and J. P. Burger, Phys. Rev. B 22, 6074 (1980).

[11]D. Misemer and B. N. Harmon (unpublished).

[12]J. H. Weaver, R. Rosei, and D. T. Peterson, Phys. Rev. B 19, 4855 (1979), I of this series of studies; and Solid State Commun. 25, 201 (1979).

[13]D. J. Peterman, B. N. Harmon, J. Marchiando, and J. H. Weaver, Phys. Rev. B 19, 4867 (1979), II of this series of studies.

[14]J. H. Weaver, D. T. Peterson, and R. L. Benbow, Phys. Rev. B 20, 5301 (1979), III of this series of studies.

[15]D. J. Peterman and B. N. Harmon, Phys. Rev. B 20, 5315 (1979), companion to Paper III.

[16]J. H. Weaver, J. A. Knapp, D. E. Eastman, D. T. Peterson, and C. B. Satterthwaite, Phys. Rev. Lett. 39, 639 (1977).

[17]J. H. Weaver and D. T. Peterson, Z. Phys. Chem. 116, 501 (1979).

[18]J. H. Weaver and D. T. Peterson, J. Less-Common Met. 74, 207 (1980); in *Metal Hydrides, 1980,* edited by G. Libowitz and G. D. Sandrock (Elsevier, Sequoia, 1980), Vol II.

[19]A preliminary report of these results was given in D. J. Peterman, D. T. Peterson, and J. H. Weaver, J. Less-Common Met. 74, 167 (1980); in *Metal Hydrides, 1980,* edited by G. Libowitz and G. D. Sandrock (Elsevier, Sequoia, 1980), Vol. II.

[20]G. Margaritondo, J. H. Weaver, and N. G. Stoffel, J. Phys. E 12, 662 (1979); see also Ref. 14.

[21]L. W. Bos and D. W. Lynch, Phys. Rev. B 2, 4567 (1979); see also Ref. 12.

[22]S. T. Manson, *The Calculation of Photoionization Cross Sections: An Atomic View,* Photoemission in Solids I, Topics in Applied Physics, edited by M. Cardona and L. Ley (Springer-Verlag, Berlin, 1978), Vol. 26.

[23]The $h\nu$ variation of the d bands within $\sim$1.5 eV of E_F can be seen in Fig. 1(a). For $h\nu \approx E_B(5p)$, the d-band cross section exhibits a minimum but is enhanced at higher photon energy, analogous to what has been observed in other metals and alloys. This arises primarily from quantum-mechanical interference between two equivalent processes, i.e., direct emission of the d state into the continuum f states, $\epsilon f\,[5p^6(6s5d)^3 + h\nu \rightarrow 5p^6(6s5d)^2 + \epsilon f]$ and the channel $5p^6(6s5d)^3 + h\nu \rightarrow 5p^5(6s5d)^4 \rightarrow 5p^6(6s5d)^2 + \epsilon f$.

[24]D. K. Finnemore (private communication).

[25]D. Khatamian, W. A. Kamitakahara, R. G. Barnes, and D. T. Peterson, Phys. Rev. B 21, 2622 (1980).

[26]D. L. Anderson, R. G. Barnes, D. T. Peterson, and D. R.

Torgeson, Phys. Rev. B 21, 2625 (1980).
[27]E. L. Venturini and P. M. Richards, Solid State Commun. 32, 1185 (1979); and E. L. Venturini, J. Appl. Phys. 50, 2053 (1979).
[28]A. C. Switendick, J. Less-Common Met. 74, 199 (1980); in *Metal Hydrides, 1980,* edited by G. Libowitz and G. D. Sandrock (Elsevier, Sequoia, 1980), Vol. II.
[29]For $YH_{1.98}$ (13.6 ± 3%) of the octahedral sites are occupied at the expense of the tetrahedral sites at $T \simeq 300$ K (Ref. 25). This may be larger for LaH_2.
[30]V. L. Moruzzi, A. R. Williams, and J. F. Janak, Phys. Rev. B 15, 2854 (1977).
[31]D. A. Papaconstantopoulos, B. M. Klein, E. C. Economou, and L. L. Boyer, Phys. Rev. B 17, 141 (1978), have shown the sensitivity of the bands of PdH to the choice of muffin-tin radii.